AGU PUBLICATIONS

Global Biogeochemical Cycles

RESEARCH ARTICLE
10.1002/2015GB005149

Key Points:
- The distribution of trace metals in waters of the global ocean was determined
- No multiyear variation in the distribution of trace metals in the Atlantic Ocean was observed
- Some metals correlate with primary productivity, suggesting potential metal limitation

Supporting Information:
- Figure S1 and Tables S1–S4

Correspondence to:
P. Pinedo-González,
pinedogo@usc.edu

Citation:
Pinedo-González, P., et al. (2015), Surface distribution of dissolved trace metals in the oligotrophic ocean and their influence on phytoplankton biomass and productivity, *Global Biogeochem. Cycles*, *29*, doi:10.1002/2015GB005149.

Received 18 MAR 2015
Accepted 15 SEP 2015
Accepted article online 23 SEP 2015

©2015. American Geophysical Union. All Rights Reserved.

Surface distribution of dissolved trace metals in the oligotrophic ocean and their influence on phytoplankton biomass and productivity

Paulina Pinedo-González[1], A. Joshua West[1], Antonio Tovar-Sánchez[2,3], Carlos M. Duarte[2,4], Emilio Marañón[5], Pedro Cermeño[6], Natalia González[7], Cristina Sobrino[5], María Huete-Ortega[5], Ana Fernández[5], Daffne C. López-Sandoval[6], Montserrat Vidal[8], Dolors Blasco[6], Marta Estrada[6], and Sergio A. Sañudo-Wilhelmy[1,9]

[1]Department of Earth Sciences, University of Southern California, Los Angeles, California, USA, [2]Department of Global Change Research, Mediterranean Institute for Advanced Studies (UIB-CSIC), Esporles, Spain, [3]Department Ecology and Coastal Management, Instituto de Ciencias Marinas de Andalucía (CSIC), Cádiz, Spain, [4]Red Sea Research Center, King Abdullah University of Science and Technology, Thuwal, Saudi Arabia, [5]Departamento de Ecología y Biología Animal, Universidad de Vigo, Vigo, Spain, [6]Institut de Ciències del Mar, Consejo Superior de Investigaciones Científicas, Barcelona, Spain, [7]Escuela Superior de Ciencias Experimentales y Tecnología, Universidad Rey Juan Carlos, Móstoles, Spain, [8]Departament d'Ecologia, Universitat de Barcelona, Barcelona, Spain, [9]Department of Biological Sciences, University of Southern California, Los Angeles, California, USA

Abstract The distribution of bioactive trace metals has the potential to enhance or limit primary productivity and carbon export in some regions of the world ocean. To study these connections, the concentrations of Cd, Co, Cu, Fe, Mo, Ni, and V were determined for 110 surface water samples collected during the Malaspina 2010 Circumnavigation Expedition (MCE). Total dissolved Cd, Co, Cu, Fe, Mo, Ni, and V concentrations averaged 19.0 ± 5.4 pM, 21.4 ± 12 pM, 0.91 ± 0.4 nM, 0.66 ± 0.3 nM, 88.8 ± 12 nM, 1.72 ± 0.4 nM, and 23.4 ± 4.4 nM, respectively, with the lowest values detected in the Central Pacific and increased values at the extremes of all transects near coastal zones. Trace metal concentrations measured in surface waters of the Atlantic Ocean during the MCE were compared to previously published data for the same region. The comparison revealed little temporal changes in the distribution of Cd, Co, Cu, Fe, and Ni over the last 30 years. We utilized a multivariable linear regression model to describe potential relationships between primary productivity and the hydrological, biological, trace nutrient and macronutrient data collected during the MCE. Our statistical analysis shows that primary productivity in the Indian Ocean is best described by chlorophyll *a*, NO_3, Ni, temperature, SiO_4, and Cd. In the Atlantic Ocean, primary productivity is correlated with chlorophyll *a*, NO_3, PO_4, mixed layer depth, Co, Fe, Cd, Cu, V, and Mo. The variables salinity, temperature, SiO_4, NO_3, PO_4, Fe, Cd, and V were found to best predict primary productivity in the Pacific Ocean. These results suggest that some of the lesser studied trace elements (e.g., Ni, V, Mo, and Cd) may play a more important role in regulating oceanic primary productivity than previously thought and point to the need for future experiments to verify their potential biological functions.

1. Introduction

Marine phytoplankton account for about half of the photosynthetic carbon fixation on Earth [*Field et al.*, 1998], thus playing a key role in the global carbon cycle and in associated climate regulation. When studying phytoplankton productivity, much of the focus is placed on the macronutrients nitrogen and phosphorus, which are known to exert a significant control on phytoplankton metabolism and community structure [e.g., *Tyrrell*, 1999; *Wu et al.*, 2000; *Ammerman et al.*, 2003; *Falkowski and Oliver*, 2007; *Moore et al.*, 2013]. However, a dozen trace elements, particularly first and second row transition metals, are also essential for the growth of phytoplankton by serving as essential active centers or structural factors in enzymes [e.g., *Morel and Price*, 2003; *Morel et al.*, 2006]. Several of these bioessential trace metals—iron (Fe), cobalt (Co), nickel (Ni), copper (Cu), cadmium (Cd), vanadium (V), and molybdenum (Mo)—are present at low concentrations in seawater, therefore possibly limiting phytoplankton production [*Da Silva and Williams*, 1993; *Moore et al.*, 2013].

In some oceanic regions, Fe availability limits both oceanic primary productivity and marine nitrogen fixation capacity [*Moore et al.*, 2009; *Saito et al.*, 2014]. Iron occurs in high amounts in the redox centers of nitrogenase

responsible for N_2 reduction to NH_3 and in various cytochromes and Fe-S redox centers involved in anoxygenic and oxygenic photosynthesis [*Saito et al*., 2011; *Sunda*, 2012]. Cobalt has been demonstrated to colimit the growth of some phytoplankton in both field and laboratory culture studies either as inorganic Co or as the central metal ion in vitamin B_{12} [*Bertrand et al*., 2007; *Taylor and Sullivan*, 2008; *Panzeca et al*., 2008]. Cobalt can also substitute for Zn in carbonic anhydrase [*Lane and Morel*, 2000a, 2000b]. Nickel serves as the active metal center in urease, a metalloenzyme involved in the assimilation of urea as a nitrogen source [*Syrett and Peplinska*, 1988; *Ermler et al*., 1998]. Nickel also serves as a cofactor in other enzymes, including hydrogenase and Ni-superoxide dismutase (Ni-SOD), an enzyme that protects organisms from oxidative stress caused by superoxide [*Mulrooney and Hausinger*, 2003; *Dupont et al*., 2008]. Copper is also an essential micronutrient. It occurs along with iron cytochrome oxidase, the terminal protein in respiratory electron transport that reduces O_2 to H_2O [*Wikström*, 2006]. It also occurs in plastocyanin, which substitutes for the iron-protein cytochrome C6 in photosynthetic electron transport in ocean diatoms [*Peers and Price*, 2006; *Sunda*, 2012]. In addition, colimitations can occur for Cu and Fe as observed in diatom cultures and batch incubation experiments [*Peers et al*., 2005; *Annett et al*., 2008; *Sunda*, 2012]. Cadmium is biologically important for marine diatoms under conditions of low Zn, as it substitutes for this metal as the metallocenter in carbonic anhydrase [*Lane and Morel*, 2000a, 2000b]. Molybdenum and V, while typically abundant in the water column with average concentrations around 100 nM [*Collier*, 1985] and 35 nM [*Dupont et al*., 1991], respectively, play important biological roles, particularly as the metal cofactors in nitrogenases and other enzymes involved in N fixation [*Kisker et al*., 1997; *Rehder*, 2000; *Crans et al*., 2004]. Zinc is required in a variety of essential proteins needed for cell growth and replication. It occurs in carbonic anhydrase [*Lindskog*, 1997], RNA polymerase [*Coleman*, 1992], involved in DNA regulation and transcription, and in tRNA synthetase [*Sankaranarayanan et al*., 2000], involved in tRNA translation into proteins.

The distributions and bioavailability of some of the bioactive trace metals discussed above have the potential to enhance or limit primary productivity and carbon export in some regions of the world ocean. Examining the link between metal distributions and phytoplankton biomass and primary productivity over basin-wide spatial scales is thus essential for understanding the controls on the biological cycles of carbon and nitrogen, including the biological transfer of carbon to the deep sea, which helps regulate atmospheric CO_2. In the last three decades, significant advances have been made in understanding the oceanic distribution of trace metals [e.g., *SCOR Working Group*, 2007]. Surface water samples collected during the Malaspina 2010 Circumnavigation Expedition (MCE) provided an opportunity to further advance the study of both the distribution of trace elements in surface waters of all major oceanic oligotrophic regions and the potential role that these micronutrients may exert on phytoplankton biomass and primary productivity.

Taking advantage of the opportunity provided by the MCE samples, this study aims to (i) determine the distribution of Co, Fe, Cd, Cu, Ni, V, and Mo in surface waters of the tropical and subtropical Atlantic, Indian, and Pacific Oceans measured during the MCE, providing new data from poorly explored and unexplored regions as well as for some understudied metals; (ii) test for changes in the distribution of some trace metals in surface waters of the Atlantic Ocean over the last 30 years; and (iii) develop empirical models describing relationships between primary productivity and the hydrological, biological, trace nutrient and macronutrient data collected during the MCE.

2. Methods

2.1. Malaspina Circumnavigation Expedition

Surface water samples were collected during the MCE aboard the R/V *Hespérides* from December 2010 to July 2011 (Figure 1 and Table S2 in the supporting information). The MCE consisted of six oceanic transects: a meridional transect from Cadiz, Spain, to Rio de Janeiro, Brazil (Stations 37–54) from December 2010 to January 2011, a transect from Brazil to Cape Town, South Africa (Stations 55–69) from January to February 2011, a transect in the Indian Ocean from South Africa to Perth, Australia (Stations 1–18) from February to March 2011, two transects in the Pacific Ocean, from Auckland, New Zealand, to Honolulu, Hawaii (Stations 70–86) from April to May 2011 and from Hawaii to Panama (Stations 87 to 110) from May to June 2011, and a final transect back to Spain across the subtropical Atlantic, from Cartagena de Indias, Colombia to Cartagena, Spain (Stations 19 to 36) from June to July 2011 (Table S2). Temperature and salinity were monitored during the cruise using a CTD (SeaBird 9 plus, Bellevue, WA, USA). The mixed layer depth (MLD) was determined from density profiles as the depth at which the density difference from the surface was 0.1 kg m^{-3}.

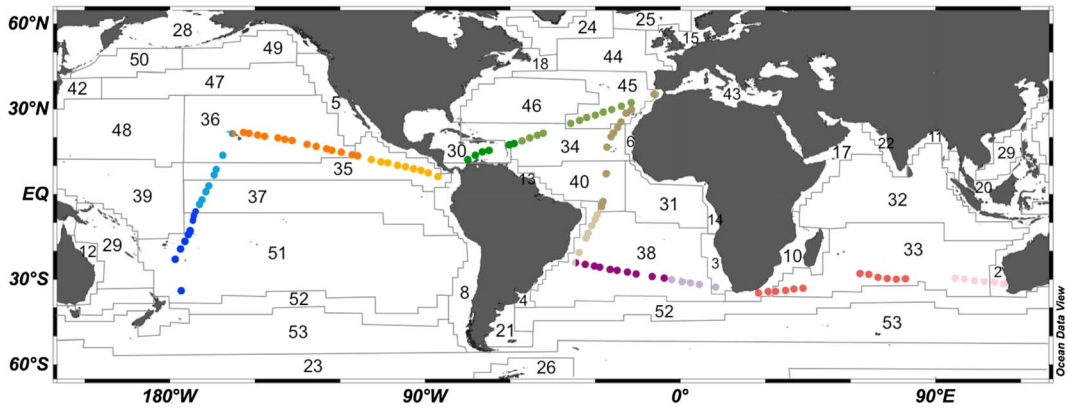

Figure 1. Map showing cruise track and Longhurst biogeochemical ocean provinces [*Longhurst*, 1998]. The provinces crossed during the MCE were the following: (2) Australia-Indonesia Coastal province, (3) Benguela Current Coastal province, (10) East Africa Coastal province, (30) Caribbean province, (33) Indian South Subtropical Gyre province, (34) North Atlantic Tropical Gyral province, (35) North Pacific Equatorial Countercurrent province, (36) North Pacific Tropical Gyre province, (37) Pacific Equatorial Divergence province, (38) South Atlantic Gyral province, (40) Western Tropical Atlantic province, (45) North Atlantic Subtropical Gyral province (east), and (51) South Pacific Subtropical Gyre province. For a complete list of provinces please refer to Table S1 in the supporting information. Colors represent the different sections used in the multivariable linear regression model. Sections were determined on the basis of distinct hydrographic and biological regimes and tested by *k*-means cluster analysis.

2.2. Collection and Analysis of Samples for Trace Metals

Samples for trace metals were collected using a teflon tow-fish sampling system deployed at approximately 3 m depth utilizing established trace metal-clean techniques [e.g., *Bruland et al*., 2005; *Berger et al*., 2008]. After sample collection, seawater was filtered on board through acid-washed 0.2 μm filter cartridges and acidified using Optima grade HCl to a pH < 2.

Dissolved samples ($<$0.2 μm) were double bagged in polyethylene bags and shipped to the trace metal clean laboratories at the University of Southern California in Los Angeles, where they were preconcentrated by an organic extraction procedure using the ammonium pyrrolidine dithiocarbamate/diethylammonium diethyldithiocarbamate (APDC/DDDC) ligand technique described in *Bruland et al*. [1985]. Levels of Fe, Cu, Cd, Mo, V, Co, and Ni were quantified by high-resolution inductively coupled plasma mass spectrometry (HR-ICP-MS) on a Thermo Element 2 HR-ICP-MS, using external calibration curves and an internal indium standard. To evaluate the accuracy of our analytical procedures, a certified seawater reference material (SRM) (CASS-5) was preconcentrated and analyzed with the samples. The recoveries of the SRM ranged from 96% for Ni to 107% for Co of the certified concentration as shown in Table S3 in the supporting information.

2.3. Collection and Analysis of Samples for Nutrients and Chlorophyll *a*

Samples for dissolved inorganic nutrients (PO_4, $NO_3 + NO_2$, SiO_4), phytoplankton biomass (as chlorophyll *a*) and primary production were collected by means of 12 L Niskin bottles mounted on a rosette frame. Samples used for dissolved nutrient analyses were drawn from the Niskin bottles into polyethylene vials and immediately frozen (−20°C) until analysis. Concentrations were measured spectrophotometrically with a Skalar autoanalyzer following standard procedures [*Grasshoff et al*., 2009; *Moreno-Ostos*, 2012]. A volume of 250–500 mL was drawn from the Niskin bottles for the total chlorophyll *a* determination, filtered through Whatman® glass microfiber filters (25 mm diameter, grade GF/F, Sigma-Aldrich, Buchs, Switzerland) and kept frozen for at least 6 h until extraction. Pigments were extracted by placing them in 5–7 mL of 90% acetone at 4°C for 24 h, and the fluorescence of the extract was determined by means of a Turner Designs fluorometer [*Yentsch and Menzel*, 1963] calibrated with a chlorophyll *a* standard (Sigma-Aldrich, Buchs, Switzerland).

2.4. Phytoplankton Productivity Measurement

Phytoplankton primary production was measured with the ^{14}C-uptake technique, following the procedures detailed in *Marañón et al*. [2000]. Samples were obtained from five depths in the euphotic layer, corresponding to 100% (3 m depth), 50%, 20%, 7%, and 1% incident PAR (photosynthetically active radiation) levels. For each depth, four 70 mL polystyrene bottles (three light bottles and one dark bottle) were filled with unfiltered seawater under dimlight conditions, inoculated with 10–20 μCi of $NaH^{14}CO_3$ and incubated inside temperature-controlled

deck incubators for 6–8 h. Appropriate irradiance levels inside each incubator were obtained by using neutral density and Blue Lagoon (Lee Filters, UK) filters. The incubation was terminated by gentle filtration (vacuum pressure < 100 mmHg) through 0.2 μm polycarbonate filters, which were then exposed to concentrated HCl fumes to remove the nonfixed, inorganic ^{14}C. After adding 5 mL of liquid scintillation cocktail to the filters, the radioactivity on each sample (disintegrations per minute (DPM)) was determined using a Wallac scintillation counter. To compute the rate of photosynthetic carbon fixation, the dark-bottle DPM value was subtracted from the light-bottle DPM value. A constant value of 25,700 $\mu g\,L^{-1}$ was assumed for the concentration of dissolved inorganic carbon. Euphotic zone-integrated values were computed by trapezoidal integration of the volumetric data down to the 1% PAR depth.

2.5. Data Interpretation

A multivariable linear regression model was used to explore correlations between oceanic primary productivity and the biogeochemical parameters measured during the MCE. Statistical work was performed in R: A language and environment for statistical computing program [*R Core Team*, 2014]. Prior to statistical analysis, the data set was subdivided into sections on the basis of distinct hydrographic and biological regimes. This hypothesis was tested via application of *k*-means cluster analysis [*R Core Team*, 2014] on the data set. Linear regression models for integrated primary productivity were constructed by employing a stepwise linear regression algorithm [*Lumley*, 2009] to exhaustively calculate polynomial regressions versus three response variables for all possible combinations of up to three variables. On the basis of R^2 and p values, statistically significant models were retained, and leave-one-out cross validation was performed to aid in selection of linear regression models that most likely reflect real trends and not data noise [*Canty and Ripley*, 2014].

3. Results and Discussion

3.1. Trace Metals, Hydrography, and Phytoplankton Productivity

Trace metal concentrations (Co, Fe, Cd, Cu, Ni, V, and Mo) varied spatially in surface waters of the world's oceans (Figures 2–7 and Table S2). Because distinct physical and biogeochemical processes influence each ocean basin, trace metal concentrations and phytoplankton properties are described separately for each region and/or transect. Integrated primary production rates were, in most stations, within the range of 10–60 $mg\,C\,m^{-2}\,h^{-1}$, which considering the photoperiod length and dark respiratory losses, is roughly equivalent to 100–600 $mg\,C\,m^{-2}\,d^{-1}$. The lowest rates of production were measured near the center of the subtropical gyres, whereas the highest values tended to occur in equatorial waters and near coastal zones.

3.1.1. Indian Ocean

Trace metals in the Indian Ocean have been poorly studied, especially in the south subtropical zone, a region with relatively complex circulation forced by the seasonal reversal of the dominant wind systems [*Longhurst*, 1998]. The MCE transect covered from South Africa to Western Australia. Samples were taken during the second half of the austral summer, in the premonsoon period (February–March). The transect conducted along the Indian Ocean crossed three distinct oceanographic regimes (Figure 1): (i) the Eastern Africa Coastal province influenced by the Agulhas current and the Agulhas Retroflection current, (ii) the Indian South Subtropical Gyre province influenced by the seasonal monsoon winds, and (iii) the Australia-Indonesia Coastal province influenced by the warm low-salinity water from the Leeuwin current [*Longhurst*, 1998; *Peterson and Stramma*, 1991; *Gordon et al.*, 1987].

3.1.1.1. Hydrography

During the MCE, the influence of warm low-salinity water from the Agulhas current and its retroflection was observed between 20 and 50°E (Figure 2a). Between 90 and 120°E, on the eastern side of the sampling transect, we detected the influence of the warm low-salinity water from the Leeuwin current. Between 50 and 90°E at the center of the Indian Ocean gyre, we observed the mixing between west gyre waters (influenced by the warm low-salinity water of the south equatorial current with salinity of 35.3) and east subtropical gyre waters (influenced by the west Australian current, with salinity of 36.2).

3.1.1.2. Surface Trace Metal Distribution and Phytoplankton Biomass and Production

In the Indian Ocean, trace metal distributions showed spatial differences along the surface transect. In general, the concentration of all measured trace metals showed enrichments near coastal zones, coincident with enhanced chlorophyll *a* and primary productivity values (Figure 2). Away from the coastal zones, in the subtropical gyre (between 85 and 105°E), pronounced surface chlorophyll *a* and integrated primary productivity maxima (of 0.13 $\mu g\,L^{-1}$ and 6.84 $mg\,C\,m^{-2}\,h^{-1}$, respectively) coincide with maxima in Cd (27 pM), Ni

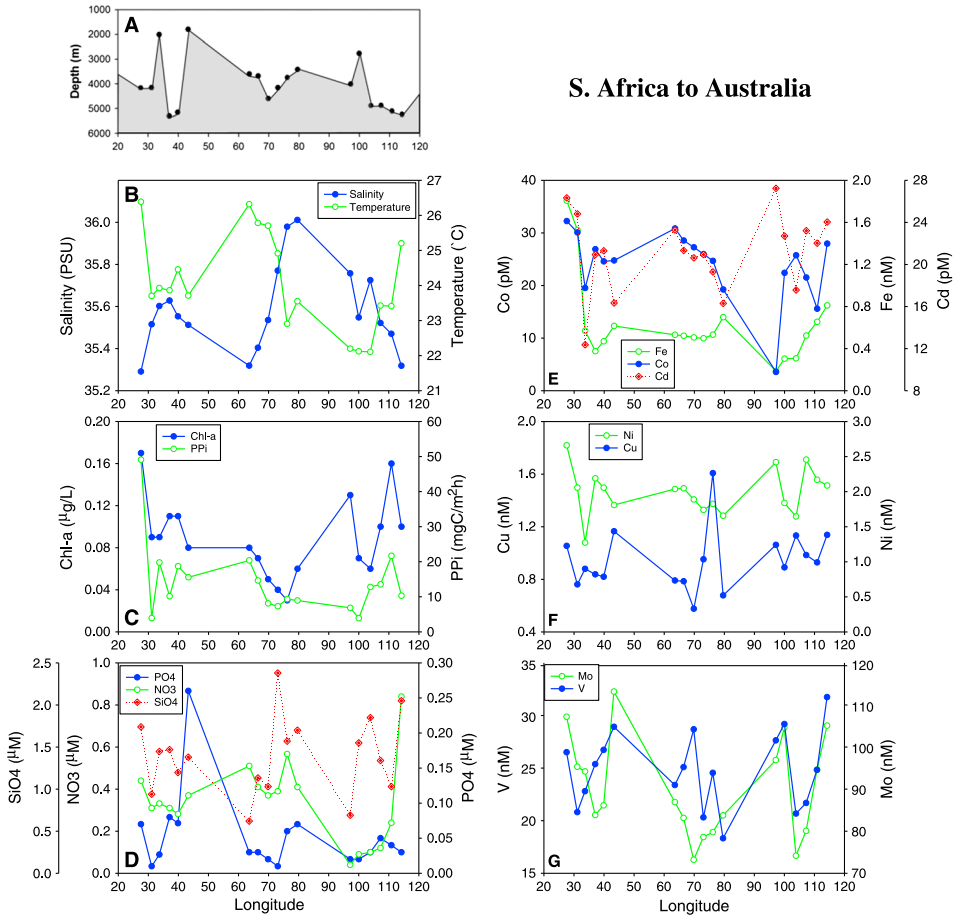

Figure 2. For the transect from South Africa to west Australia in the Indian Ocean, surface water distributions are shown for (a) depth, (b) salinity and temperature, (c) chlorophyll *a* (Chl *a*) and depth-integrated primary productivity (PPi), (d) NO_3, SiO_4, and PO_4, (e) cobalt, iron, and cadmium, (f) copper and nickel, and (g) vanadium and molybdenum.

(2.5 nM), Mo (106 nM), and V (29 nM) concentrations as well as minima in Fe (0.18 nM), Co (3 pM), and the inorganic nutrients PO_4 (0.02 µM) and NO_3 (0.05 µM) (Figure 2). The enhanced biological productivity observed at this location is probably due to detached cyclonic eddies developed from the Leeuwin current, containing higher levels of chlorophyll *a* biomass and coastal phytoplankton communities (Figure S1) [*Griffin et al.*, 2001; *Moore et al.*, 2007; *Feng et al.*, 2007].

Across the Indian Ocean transect, dissolved Mo, V, and Cu ranged from 70 to 110 nM, 18 to 32 nM, and 0.6 to 1.6 nM, respectively, with none of these elements displaying a clear longitudinal trend (Figures 2e and 2f). Dissolved Cd, Co, and Ni ranged from 12 to 26 pM, 5 to 32 pM, and 1.2 to 2.5 pM, respectively. Between 60 and 80°E, in the oligotrophic gyre, these metals showed an excellent negative correlation with salinity ($R^2 = 0.74$, 0.80, and 0.80, respectively, $p < 0.05$) suggesting that the geographical distributions observed for these trace elements were influenced by water mass mixing: the west gyre waters influenced by the warm low-salinity water of the south equatorial current with relatively high metal concentrations (probably due to wet deposition at the intertropical convergence zone (ITCZ)) mixing with the cold, high-salinity, metal-depleted waters of the east subtropical gyre (Figures 2d and 2e).

Indian Ocean dissolved Fe concentrations ranged from 0.18 nM in the oligotrophic gyre to 1.8 nM at the coastal zone off South Africa. No longitudinal trend was observed for this metal other than enhanced values at the extreme eastern and western boundaries of the sampling transect (Figure 2d).

3.1.2. Atlantic Ocean

The Atlantic Ocean is perhaps the best-studied ocean basin in the world, particularly in the case of the North Atlantic. However, much of the prior attention has focused on the distribution of Fe due to its

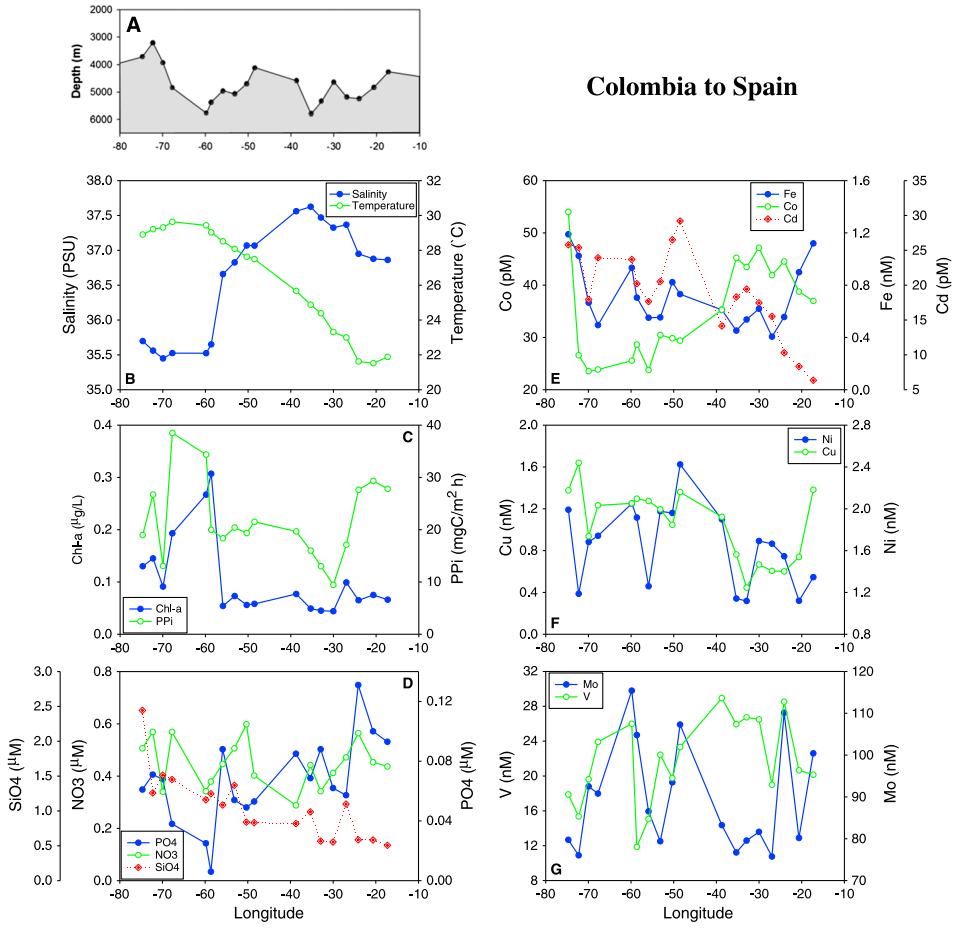

Figure 3. For the transect from Colombia to Spain in the Atlantic Ocean, surface water distributions are shown for (a) depth, (b) salinity and temperature, (c) chlorophyll *a* (Chl *a*) and depth-integrated primary productivity (PPi), (d) NO_3, SiO_4, and PO_4, (e) cobalt, iron, and cadmium, (f) copper and nickel, and (g) vanadium and molybdenum.

importance in regulating oceanic primary productivity. In comparison, relatively little is known about the regional distribution of metals like V, Mo, Co, Cd, Cu, and Ni in the Atlantic. Therefore, samples collected during the MCE provide an excellent opportunity to build on the work of previous oceanographic campaigns and improve our understanding of some understudied trace elements. The Atlantic Ocean sampling campaign was divided into three transects: Colombia to Spain (June–July 2011), Spain to Brazil (December 2010 to January 2011), and Brazil to South Africa (January–February 2011) (Figure 1). In particular, trace metal samples collected along two understudied transects in the Atlantic Ocean (Colombia to Spain and Brazil to South Africa, Figure 1) provide new information about the distribution of trace elements in this ocean basin.

3.1.2.1. Hydrography

3.1.2.1.1. Colombia to Spain Transect

The longitudinal transect that started in Cartagena de Indias, Colombia, and ended in Cartagena, Spain, crossed three distinct biogeochemical ocean provinces (Figure 1): (i) the Caribbean province influenced by the North Brazil current and the north equatorial current, (ii) the North Atlantic Tropical Gyre province where the lowest surface chlorophyll *a* values of the North Atlantic are usually found, and (iii) the North Subtropical Gyre province influenced by the Canary current [*Longhurst*, 1998].

Samples were collected in late May to early June, when the North Equatorial Counter current surface flow is discontinuous and North Brazil current waters (chemically modified by the Amazon and Orinoco River waters) enter the province between Trinidad and Barbados [*Farmer et al.*, 1993; *Longhurst*, 1998]. The influence of this warm (28°C) low-salinity (35.7) water is observed in the western side of the sampling transect between 60° and 80°W (Figure 3a). On the eastern side of the sampling section between 15° and 25°W, the influence of

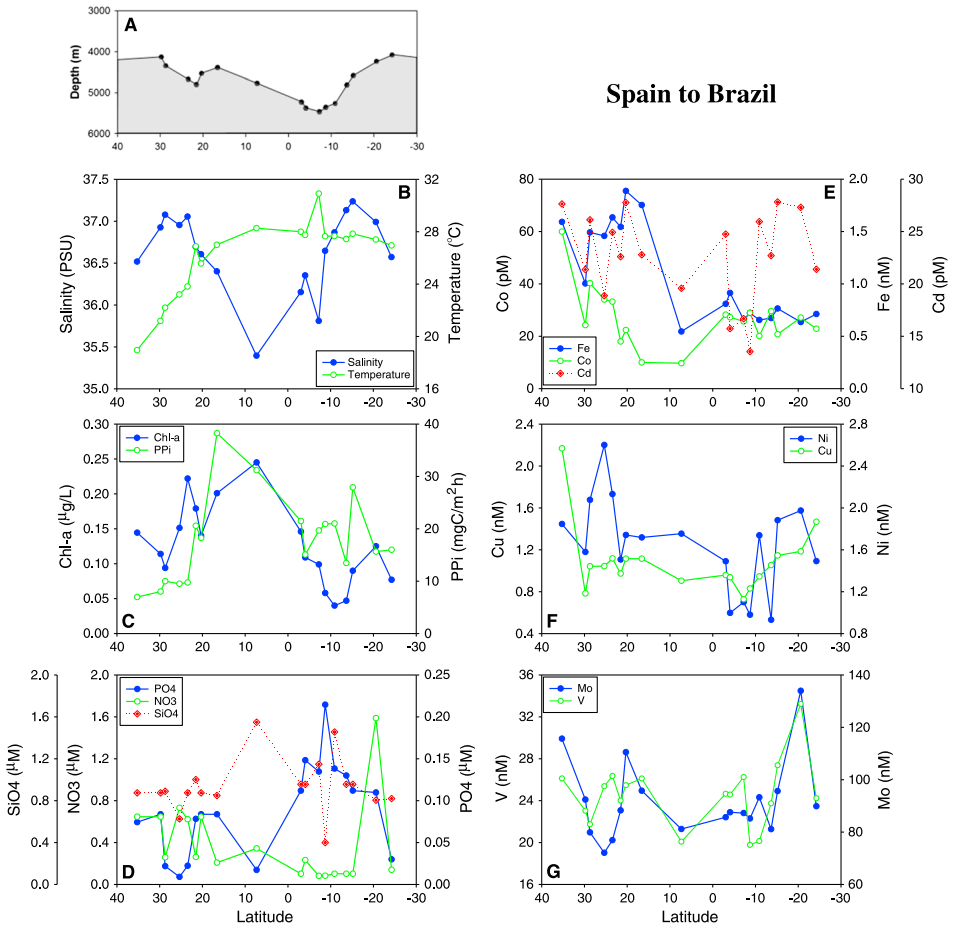

Figure 4. For the transect from Spain to Brazil in the Atlantic Ocean, surface water distributions are shown for (a) depth, (b) salinity and temperature, (c) chlorophyll *a* (Chl *a*) and depth-integrated primary productivity (PPi), (d) NO_3, SiO_4, and PO_4, (e) cobalt, iron, and cadmium, (f) copper and nickel, and (g) vanadium and molybdenum.

relatively cold (21°C) high-salinity (36.8) water from the Canary current is observed. The center of the North Atlantic tropical gyre (25 to 80°W) seems to be a mixture of these two distinct water masses (Figure 3a).

3.1.2.1.2. Spain to Brazil

The transect that started in Cadiz, Spain, and ended in Rio de Janeiro, Brazil, covered four different biogeochemical ocean provinces (Figure 1): (i) the North Subtropical Gyre province, (ii) the North Atlantic Tropical Gyre province, (iii) the Western Tropical Atlantic province influenced by the seasonally varying strength and position of the hemispheric trade winds and the ITCZ, and (iv) the South Atlantic Gyral province (west), influenced by the Brazil and south equatorial currents [*Peterson and Stramma*, 1991; *Longhurst*, 1998].

The influence of relatively cold (18–22°C) high-salinity (36.5–37) waters from the Canary current is observed in the northern part of the sampling transect between 24 and 35°N (Figure 4a). The rest of the transect maintains a roughly constant temperature of about 28°C (Figure 4a) suggesting the southward flow of this water mass and subsequent mixing with warmer waters from the north and south equatorial currents and ultimately with the warm subtropical waters of the Brazil current [*Peterson and Stramma*, 1991; *Longhurst*, 1998]. In contrast, salinity values dropped between 15°N and 5°S latitude (Figure 4a) consistent with high net precipitation caused by the ITCZ at those latitudes [*Peterson and Stramma*, 1991; *Bigg*, 2003].

3.1.2.1.3. Brazil to South Africa

The sampling transect that began in Brazil and ended in Cape Town, South Africa, encompasses only one biogeochemical ocean province (Figure 1), the South Atlantic Gyral province, influenced by the coastal boundary currents of Brazil and Benguela [*Longhurst*, 1998]. The hydrographic conditions observed during this transect seem to reflect the interaction between the warm (27°C) high-salinity (36.6) waters that dominate the western side of the South Subtropical Gyre and the relatively cold (20°C) low-salinity (35.5) waters from the

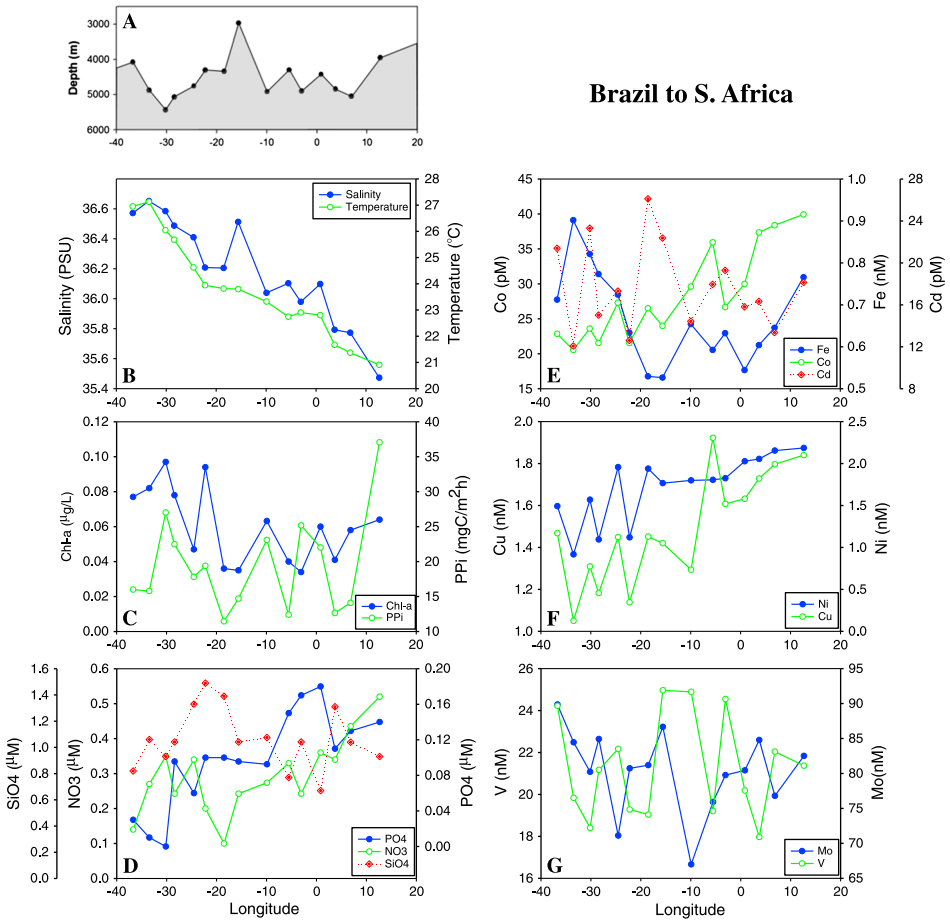

Figure 5. For the transect from Brazil to South Africa in the Atlantic Ocean, surface water distributions are shown for (a) depth, (b) salinity and temperature, (c) chlorophyll *a* (Chl *a*) and depth-integrated primary productivity (PPi), (d) NO_3, SiO_4, and PO_4, (e) cobalt, iron, and cadmium, (f) copper and nickel, and (g) vanadium and molybdenum.

South Atlantic current (Figure 5a). The observed salinity and temperature trends between Brazil and South Africa seem to be the result of mixing between these water masses.

3.1.2.2. Surface Trace Metal Distribution and Phytoplankton Biomass and Production

3.1.2.2.1. Colombia to Spain

In this region of the Atlantic Ocean we observed trace metal concentration enrichments near coastal areas (Figures 3d–3f). In the Caribbean province, between 70 and 55°W, pronounced surface water chlorophyll *a* and integrated primary productivity maxima of 0.3 $\mu g\,L^{-1}$ and 38 $mg\,C\,m^{-2}\,h^{-1}$, respectively, coincide with maxima in V (26 nM) and Mo (115 nM) concentrations as well as minima in Co (23 pM) and PO_4 (0.03 μM) (Figures 3b–3f).

Dissolved Fe and Ni ranged from 0.4 to 1.2 nM and 1.1 to 2.4 nM, respectively, with neither element displaying a clear longitudinal trend other than enhanced Fe values at the eastern and western sections of the transect, in environments influenced by land proximity (Figures 3d and 3e).

Dissolved Cd and Cu ranged from 6.3 to 29 pM and 0.4 to 1.6 nM, respectively. Both metals showed a similar trend, with the highest levels detected between 80 and 45°W in the Caribbean province and decreasing concentrations toward the eastern side of the transect, with the lowest values measured between 40 and 20°W (Figures 3d and 3e). In the case of Cu, however, high concentrations of this metal were measured at the easternmost station. Dissolved V and Mo ranged from 12 to 28 nM and 75 to 115 nM, respectively. Between 70 and 45°W within the Caribbean province, their maximum values coincide with the highest levels of phytoplankton biomass (as chlorophyll *a*) and primary productivity (Figure 3f). Dissolved Co concentration was 55 pM in the coastal zone off Colombia while in the rest of the Caribbean province, Co concentrations were around 25 pM. The lowest Co levels were measured between 72°W and 50°W longitude, coinciding with maxima in both chlorophyll *a* and primary productivity values.

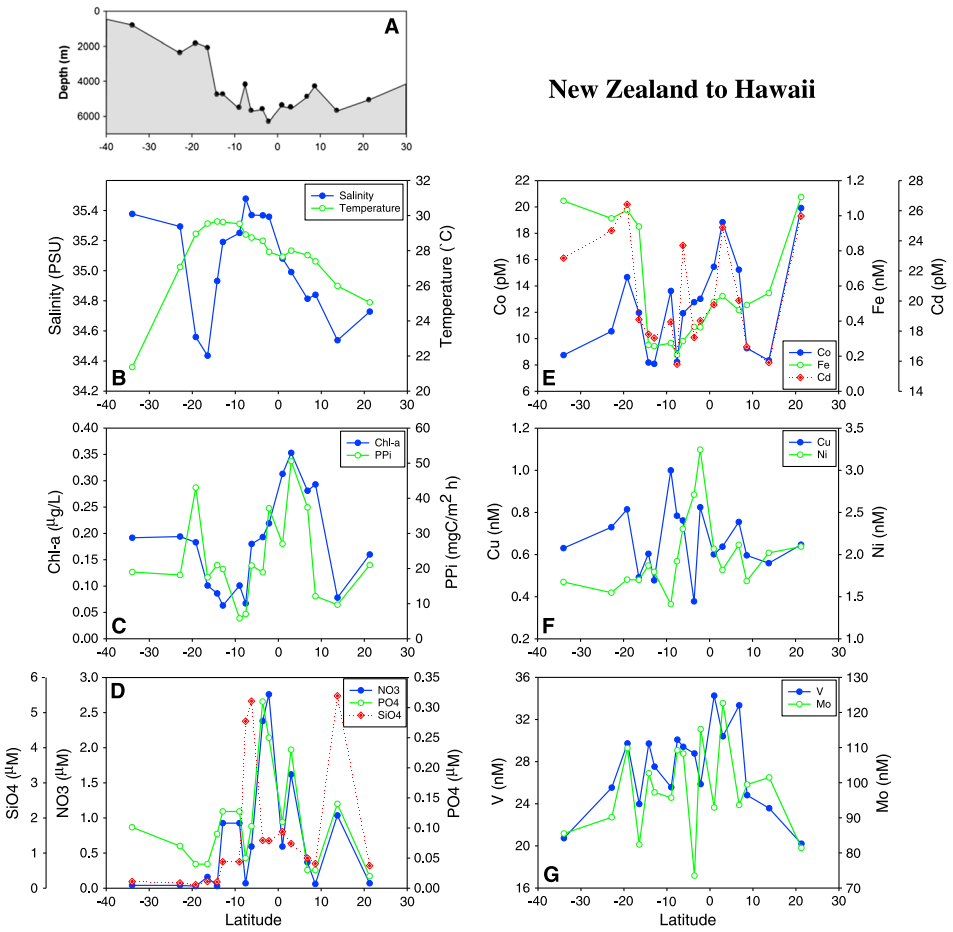

Figure 6. For the transect from New Zealand to Hawaii in the Pacific Ocean, surface water distributions are shown for (a) depth, (b) salinity and temperature, (c) chlorophyll *a* (Chl *a*) and depth-integrated primary productivity (PPi), (d) NO_3, SiO_4, and PO_4, (e) cobalt, iron, and cadmium, (f) copper and nickel, and (g) vanadium and molybdenum.

3.1.2.2.2. Spain to Brazil

The distribution of trace metals in surface waters of this latitudinal transect showed distinct regional features (Figure 4). Between 20°N and 3°S, pronounced chlorophyll *a* and primary productivity maxima of 0.24 µg L^{-1} and 31 mg C m^{-2} h^{-1}, which reflect the effect of the Mauritanian and equatorial upwelling regions [*Marañón et al.*, 2000], coincided with a maximum in SiO_4 (1.55 µM) concentration and minima in Co (10 pM), Fe (0.5 nM), V (20 nM), and PO_4 (0.02 µM) (Figures 4b–4f).

Dissolved Cd, Mo, and V ranged from 14 to 28 pM, 70 to 135 nM, and 20 to 33 nM, respectively, and none of these elements displayed a clear latitudinal trend (Figures 4d–4f). Concentrations of Co and Fe ranged from 10 to 60 pM and 0.5 to 1.8 nM, respectively. The highest levels of both elements were measured in the northern part of the transect, decreasing southward (Figure 4d). This geographical trend is probably due to dust deposition, which is higher in the North Atlantic downwind from the Sahara, decreasing rapidly south of the ITCZ [*Bristow et al.*, 2010; *Ridley et al.*, 2012].

Dissolved Cu ranged from 1.6 to 2.2 nM. No latitudinal trend is displayed by concentrations of this metal other than enhanced values at the extreme north and south parts of the transect (Figure 4e). Dissolved Ni concentration ranged from 0.9 to 2.4 nM, and although no clear latitudinal trend is observed for this metal, the variation follows closely that of chlorophyll *a* (Figures 4b and 4e).

3.1.2.2.3. Brazil to South Africa

The highest levels of dissolved Fe (0.7 nM), Co (40 pM), Ni (2.1 nM), Cu (1.8 nM), and NO_3 (0.5 µM) along this transect were measured off the coast of South Africa (Figures 5c–5e). These high values coincide with areas

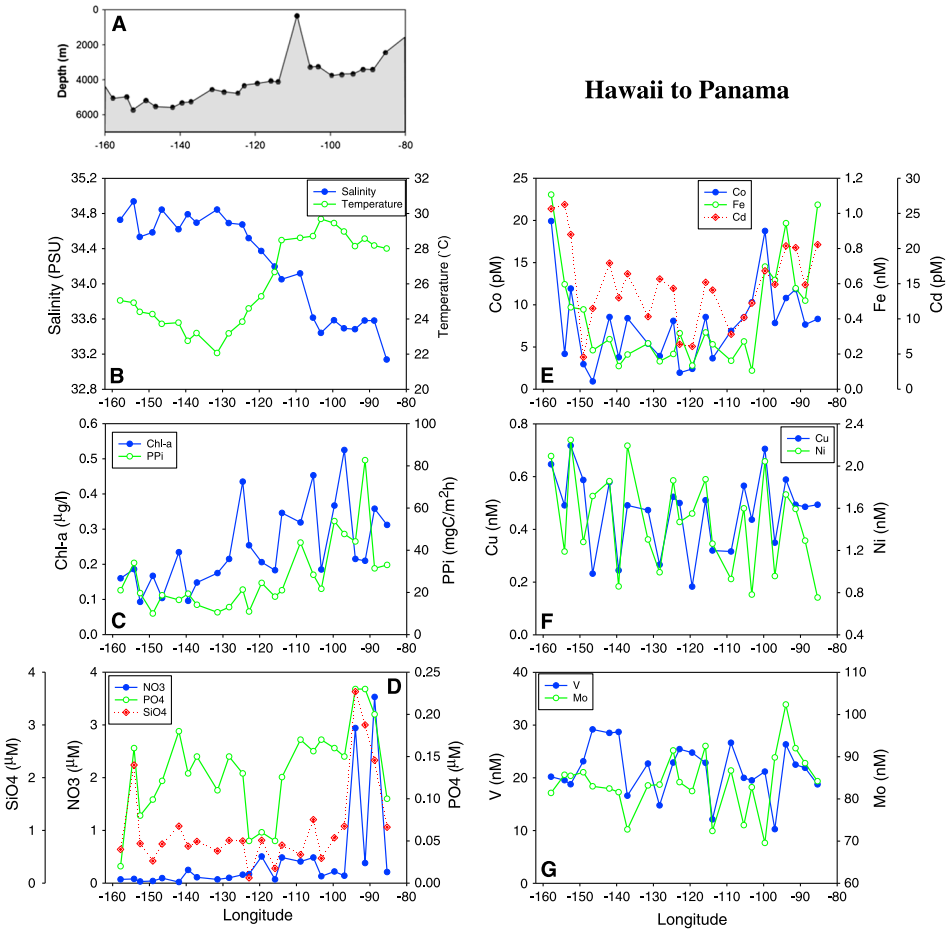

Figure 7. For the transect from Hawaii to Panama in the Pacific Ocean, surface water distributions are shown for (a) depth, (b) salinity and temperature, (c) chlorophyll *a* (Chl *a*) and depth-integrated primary productivity (PPi), (d) NO_3, SiO_4, and PO_4, (e) cobalt, iron, and cadmium, (f) copper and nickel, and (g) vanadium and molybdenum.

of enhanced primary productivity (37 mg C m^{-2} h^{-1}) probably due to the influence of the nutrient-rich waters from the Benguela current (Figure 5b).

The distribution of dissolved Co, Cu, and Ni ranged from 23 to 40 pM, 1.1 to 1.8 nM, and 1.0 to 2.1 nM, respectively, and their spatial distribution was inversely related to both surface salinity and temperature (Figure 5a). Minimum values were found in the western side of the oligotrophic gyre and maximum values in the eastern side of the transect (Figures 5d and 5e). Dissolved Fe concentrations ranged from 0.5 to 0.9 nM, and no longitudinal trend was observed for this metal other than higher values in the western side of the gyre and off the coast of South Africa (Figure 5d). Similarly, dissolved Cd, V, and Mo concentrations, which ranged from 18 to 42 pM, 18 to 25 nM, and 67 to 90 nM, respectively, did not show a clear longitudinal trend (Figures 5d and 5f).

3.1.3. Pacific Ocean

The Pacific Ocean is the world's largest ocean basin, with about 165.25 million square kilometers in area, covering one third of Earth's total surface area. Accurate data on the distribution of trace metals in the surface waters of the Pacific Ocean have been generated over many years [e.g., *Boyle et al.*, 1977; *Bruland*, 1980; *Nürnberg et al.*, 1983; *Bruland et al.*, 1994; *Boyle et al.*, 2005; *Blain et al.*, 2008; *Slemons et al.*, 2010]. However, it is not surprising that many areas of this vast ocean basin remain understudied or have not been studied at all, especially regarding trace metal concentrations. Dissolved Co, Fe, Cd, Cu, Ni, V, and Mo concentrations measured in the MCE provide a new data set that improves our understanding of the distribution of trace metals in this ocean basin. Samples were collected along two transects in the Pacific Ocean: from Auckland, New Zealand, to Honolulu, Hawaii, (April–May 2011) and from Hawaii to Panama (May–June 2011).

3.1.3.1. Hydrography

3.1.3.1.1. New Zealand to Hawaii

The latitudinal transect from New Zealand to Hawaii crossed three different biogeochemical ocean provinces (Figure 1): (i) the South Subtropical Gyre province, which may be the most uniform and seasonally stable region of the open ocean, (ii) the Pacific Equatorial Divergence province that encompass the nitrate-replete waters of the eastern tropical Pacific, and (iii) the North Pacific Tropical Gyre province, where curls due to wind stress form eddies that induce upwelling and downwelling off the Hawaiian Islands [*Longhurst*, 1998; *Jia et al*., 2011].

Most of the sampling sites along this transect were located within the tropics. Consequently, the temperature measured at the stations between 19°S and 7°N was fairly constant, oscillating between 27.7 and 29.6°C (Figure 6a). In contrast, samples collected at the southernmost site (34°S) were located in colder water (21°C) influenced by the Antarctic Circumpolar current. The influence of the South Pacific convergence zone (SPCZ) is observed between 20° and 10°S, where salinity levels drop from 35.2 to 34.4 (Figure 6a). Between 10°S and 1°N, east of the SPCZ, a surface salinity maximum is formed due to a positive evaporation-precipitation balance [*Donguy*, 1994]. The influence of the ITCZ is observed at the northernmost part of the transect, south of the Hawaiian Islands between 2 and 15°N, where salinity declines from the tropical salinity maximum value of 35.5 to 34.6 (Figure 6a).

3.1.3.1.2. Hawaii to Panama

The longitudinal transect that started in Hawaii and ended in Panama covered two different biogeochemical ocean provinces (Figure 1): (i) the North Pacific Tropical Gyre province influenced by the North Equatorial and California current systems as well as by the effect of the Hawaiian Islands and (ii) the North Pacific Equatorial Countercurrent province, influenced by the quasi-permanent cyclonic feature, the Costa Rica dome [*Umatani and Yamagata*, 1991; *Longhurst*, 1998].

The distribution of salinity at the surface shows maximum values of 35 around the coast of Hawaii at about 157°W (Figure 7a). These high-salinity values are likely due to the influence of waters flowing from the subtropical salinity maximum [*Talley et al*., 2011]. In the middle of the sampling transect (around 105°W), salinity values start decreasing probably due to the influence of heavy precipitation in the vicinity of the ITCZ [*McClymont et al*., 2012]. Values keep decreasing eastward, where a minimum is observed between 85 and 88°W (Figure 7a). The occurrence of this low-salinity water at the farthest east side of the transect is probably due to local coastal precipitation, as it has been shown that during the rainy season, from May to November, such low-salinity water is confined to coastal areas [*Peterson*, 1960].

3.1.3.2. Surface Trace Metal Distribution and Phytoplankton Biomass and Production

3.1.3.2.1. New Zealand to Hawaii

Close to the equator, between 5°S and 5°N, we observed pronounced primary productivity and chlorophyll *a* maxima of 50 mg C m^{-2} h^{-1} and 0.35 μg L^{-1}, respectively, which coincided with maxima in concentrations of Co, Cd, Ni, V, and Mo concentrations (19 pM, 25 pM, 3.2 nM, 34 nM, and 120 nM, respectively) and the macronutrients NO_3, PO_4, and SiO_4 (2.7 μM NO_3, 0.3 μM PO_4, and 5.3 μM SiO_4) (Figure 6). The enhanced biological productivity and the high macronutrient and trace-nutrient levels are probably due to the influence of equatorial upwelling that replaces the warm nutrient-depleted surface waters with denser, cooler, nutrient-rich waters from below [*Talley et al*., 2011]. Along this transect, dissolved Co, Cd, Ni, Cu, Mo, and V ranged from 8 to 20 pM, 16 to 26 pM, 1.5 to 3.3 nM, 0.5 to 3.3 nM, 80 to 120 nM, and 20 to 34 nM, respectively, although none of these elements displayed a clear longitudinal trend (Figures 6d–6f).

Dissolved Fe concentration along this transect ranged from 0.2 to 1.1 nM. No latitudinal trend was observed for Fe other than higher values at the northern and southern ends of the transect (Figure 6d). Although Fe levels are low (<0.5 nM) around the equator at about 13°S to 10°N, the lowest concentrations are found in the Southern Hemisphere at about 5°S (0.2 nM), increasing steadily toward the north. This trend agrees well with the process suggested by *Duce and Tindale* [1991], in which African dust from the desertification of the Sahel is carried into the Caribbean and across the Isthmus of Panama, depositing 1–10 mg Fe m^{-2} yr^{-1} onto the surface of the Pacific Equatorial Divergence province just north of the equator (Figure 1). There is also direct evidence that in this province the trade winds of the Northern Hemisphere carry a significantly higher concentration of mineral dust than the trades of the Southern Hemisphere [*Maenhaut et al*., 1983], potentially enhancing Fe, chlorophyll *a*, and primary productivity values in the Pacific Ocean between 5° and 8° N (Figure 6c).

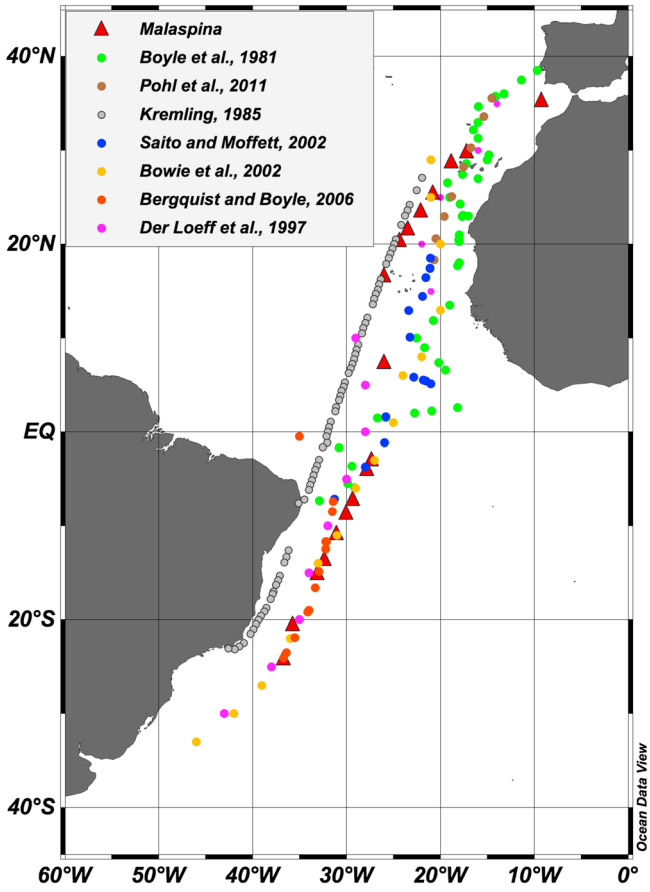

Figure 8. Map showing the cruise tracks of eight different oceanographic campaigns (including MCE, reported in this study) in the Atlantic Ocean basin along the Spain to Brazil transect.

3.1.3.2.2. Hawaii to Panama

The divergent upwelling effect at the Costa Rica dome in the eastern part of this transect causes the transport of the tropical thermocline (and its associated nutricline) to the surface in the center of the dome with significant biological consequences [*Umatani and Yamagata*, 1991]. This effect is observed between 100° and 80°W as pronounced surface water primary productivity and chlorophyll *a* maxima of 82 mg C m^{-2} h^{-1} and 0.5 μg L^{-1}, respectively, which coincide with maxima in Fe (0.9 nM), Cd (20 pM), and Mo (102 nM) and nutrients NO_3 (3.5 μM), PO_4 (0.2 μM), and SiO_4 (3.6 μM) (Figure 7).

As observed in other regions of the world oceans, dissolved Cu, Ni, V, and Mo ranged from 0.2 to 0.7 nM, 0.8 to 2.2 nM, 10 to 30 nM, and 70 to 105 nM, respectively, with none of these elements displaying a clear longitudinal trend (Figures 7e and 7f).

Dissolved Co, Fe, and Cd ranged from 1 to 20 pM, 0.1 to 1.1 nM, and 5 to 25 pM respectively. No longitudinal trend is displayed by these metals other than enhanced values off the coast of Hawaii and between 100° and 85°W, the area affected by the Costa Rica dome (Figure 7d).

3.2. Temporal Changes in Trace Metal Concentrations in the Surface Atlantic Ocean

Since the advent of trace metal clean techniques, trace metal distributions have been established for vast areas of the ocean, in particular the Atlantic Ocean. The data derived from samples collected along the Spain to Brazil transect (Figure 1) provide the opportunity to explore temporal variability in the distribution of trace metals in surface waters of the Atlantic Ocean by comparing our results with some of those measured along the same section over the last 30 years. In this analysis, our goal is not to provide a comprehensive survey of prior work but rather to put our results in context—both demonstrating the quality of our data and providing an opportunity to consider temporal trends for one restricted region by focusing attention on a set of previously published studies that covered the most similar region to our own Atlantic transect.

A comparison of the salinity measured between Spain and Brazil in December 2010 and January 2011 during the MCE and that measured in the same area in 1978 [*Boyle et al.*, 1981], 1980 [*Kremling*, 1985], 1989 [*Pohl et al.*, 2011], 1990 [*Van Der Loeff et al.*, 1997], and 2002 [*Saito and Moffett*, 2002; *Bowie et al.*, 2002] (Figure 8) show that the hydrographic conditions in surface waters of the Atlantic Ocean are statistically similar (Figures 9a and 9b). The fact that surface salinity levels in this area of the ocean have remained relatively unchanged over the last 30 years suggests that the physical processes influencing this area of the Atlantic Ocean (e.g., water mass composition/structure and general circulation) have also remained relatively steady. Therefore, any changes in trace metal levels in our temporal comparison are most likely due to fluctuation in the inputs and outputs of metals.

Dissolved Co concentrations measured during the MCE, plotted in Figure 9c as a function of latitude along with data from four other Atlantic cruises [*Pohl et al.*, 2011; *Bowie et al.*, 2002; *Berquist and Boyle*, 2006], did not exhibit statistical differences with respect to previously published data (Figure 9d). These similarities

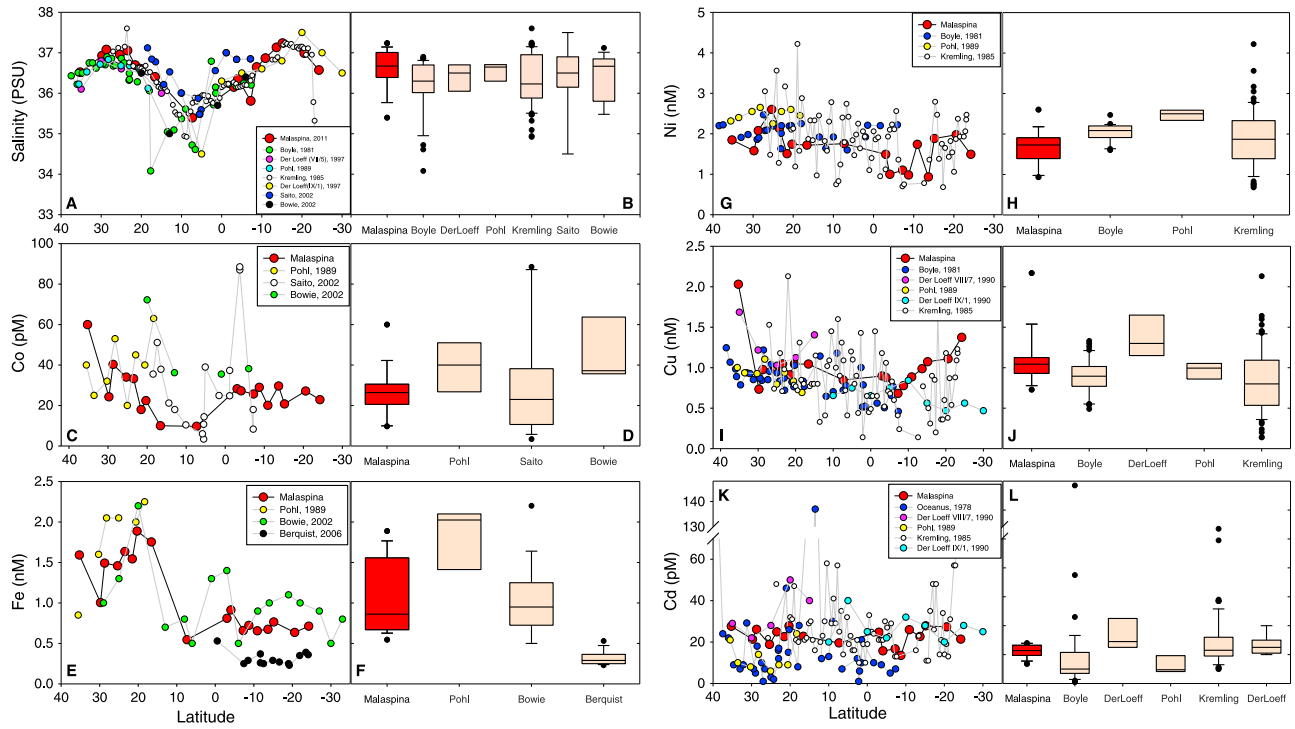

Figure 9. Surface water distributions and box-and-whiskers plot comparison of measured (a and b) salinity, (c and d) cobalt, (e and f) iron, (g and h) nickel, (i and j) copper, and (k and l) cadmium with literature data for the transect from Spain to Brazil. Boxes encompass values between the 25th and 75th percentiles, whiskers give the 95% range of values, and lines in the box represent the median values of the distribution. Solid circles represent outliers, which are values above 1.5 times the length of the box.

suggest that in this part of the Atlantic Ocean (Figure 8), the balance of Co inputs and outputs has remained relatively invariant over the last 30 years. The same unchanged temporal trend can be observed for Cu, Ni, and Cd (Figures 9g–9l). In the case of Fe, concentrations measured on the MCE samples are between the range reported by *Pohl et al.* [2011] for samples collected in 1989 and *Bowie et al.* [2002] for samples collected in 1996 (Figures 9e and 9f). However, Fe concentrations were on average 0.3 nM higher in 2011 at the MCE sampling sites (median = 0.6 nM) than the levels reported by *Bergquist and Boyle* [2006] (median = 0.3 nM) (Figures 9e and 9f). The differences might be attributed to the season in which the samples were collected, as pulses of northeast winds that draw South Atlantic Central water to the surface occur more frequently during the austral spring-summer (when the MCE samples were collected) than in autumn-winter (when the *Bergquist and Boyle* [2006] samples were collected). Although both sets of samples were collected approximately 200 km away from the upwelling-downwelling zone of Cape Frio, the influence of upwelling is observed more in the MCE samples as suggested by the higher concentrations of Fe, Cd, NO_3, and PO_4 (Figures 3c and 3d).

In general, the distribution of metals measured in the latitudinal transect between Spain and Brazil during the MCE agrees well with metal levels reported in the literature (Figure 9). This leads to the conclusion that the balance of inputs and outputs for most trace metals has remained relatively unchanged in this part of the world ocean over the last 30 years.

3.3. Effect of Trace Metals, Hydrography, and Macronutrients on Phytoplankton Biomass and Productivity

We utilized a modeling approach to describe potential relationships between primary productivity and the hydrological, biological, trace-nutrient and macronutrient data collected during the MCE (Table S2). We used a multivariable linear regression model (equation (1)) to identify the variables within the sample set that best correlate with the observed primary productivity in each ocean basin, as follows:

$$\text{Primary Productivity} = C_0 + C_1X_1 + C_2X_2 + C_3X_3 \quad (1)$$

where C_n are the regression weights, computed in a way that minimizes the sum of squared deviations, and X_n are the independent variables (e.g. trace metal concentrations).

Table 1. Best Fit Linear Models and Diagnostic Statistics for Primary Productivity for the Ocean Basins and Transects Sampled During the MCE[a]

Ocean Basin	Transect	Section	Model Variables	R^2	p	PE
Indian Ocean	South Africa to Australia	1	Chl a + NO_3 + Ni	0.86	0.001	0.03
		2	Temp + SiO4 + Cd	1.00	0.001	0.09
Atlantic Ocean	Colombia to Spain	1	NO_3 + V + Mo	0.97	0.045	0.00
		2	Chl a + PO_4 + Fe	0.76	0.007	0.24
	Spain to Brazil	1	NO_3 + Co + Cu	0.94	0.000	0.25
		2	MLD + Co + Fe	0.97	0.007	0.03
	Brazil to South Africa	1	MLD + Chl a + Co	0.94	0.001	0.07
		2	Co + Cd + NO_3	0.94	0.036	0.00
Pacific Ocean	Hawaii to Panama	1	SiO_4 + NO_3 + Cd	0.78	0.001	0.14
		2	Salinity + NO_3 + Cd	0.92	0.004	0.32
	NZ to Hawaii	1	PO4 + Fe + V	0.84	0.020	0.46
		2	Temp + Fe + Cd	0.97	0.002	0.18

[a]Different sections are shown in Figures 1 and 10.

Linear regression models were constructed using a stepwise linear regression algorithm [*Lumley*, 2009] and validated by a leave-one-out cross-validation method [*Canty and Ripley*, 2010] to minimize over fitting. After the validation step, the best fit model was determined by the highest R^2, lowest p value, and lowest predictive error. Best fit models and relevant statistical metrics for all six MCE transects are presented in Table 1, summarized in Table 2, and plotted versus observed field data in Figure 10.

The best fit model for primary productivity for the transect from South Africa to Australia involves chlorophyll a, NO_3, and Ni for the western section and temperature, SiO_4 and Cd for the eastern side of the transect (Table 1 and Figure 10a). For the transect from Colombia to Spain, primary productivity is best predicted by NO_3, V, and Mo for the western part and chlorophyll a, PO_4 and Fe for the eastern side of the transect (Table 1 and Figure 10b). From Spain to Brazil, the best fit model identifies Co as an important independent variable in the entire transect, while NO_3 and Cu were significant for the northern section, and Fe and mixed layer depth (MLD) for the southern part of the transect (Table 1 and Figure 10c). From Brazil to South Africa, the model shows the relevance of Co for the entire transect, and chlorophyll a and MLD for the western section, while Cd and NO_3 were important variables for the eastern side of the transect (Table 1 and Figure 10d). The model for the transect from Hawaii to Panama includes NO_3 and Cd concentrations for the entire transect, SiO_4 for the western section, and salinity for the eastern part of the transect (Table 1 and Figure 10e). The best fit model for primary productivity along the transect from New Zealand to Hawaii includes Fe concentrations for the entire transect, PO_4 and V for the southern section, and temperature and Cd for the northern section (Table 1 and Figure 10f).

The multivariable linear regression approach allows us to explore correlative relationships among the independent variables that could influence surface biomass along the MCE cruise. However, among other shortcomings, a major conceptual limitation of linear regression models is that they do not identify the underlying causal mechanisms responsible for the observed correlations. With this in mind, a functional discussion of the multivariable linear model outcome is presented below, particularly considering the extent to which our model results are consistent with field and laboratory observations reported in the literature.

Table 2. Table Summarizing the Variables and Correlation Type (Positive or Negative) Identified in the Best Fit Models Describing Productivity for All the Ocean Basins and Transects Sampled During the MCE

Ocean Basin	Transect	Salinity	Temperature	Chl a	SiO_4	NO_3	PO_4	Co	Fe	Cd	Cu	Ni	V	Mo	MLD[a]
Indian Ocean	South Africa to Australia		+	+	-	+				-		-			
Atlantic Ocean	Colombia to Spain			+		+	+		+				+	+	
	Spain to Brazil					-		-	+		+				+
	Brazil to South Africa			+		+		+		+					+
Pacific Ocean	Hawaii to Panama	+			+	-				+					
	New Zealand to Hawaii		-				+		-	+			+		

[a]Mixed layer depth.

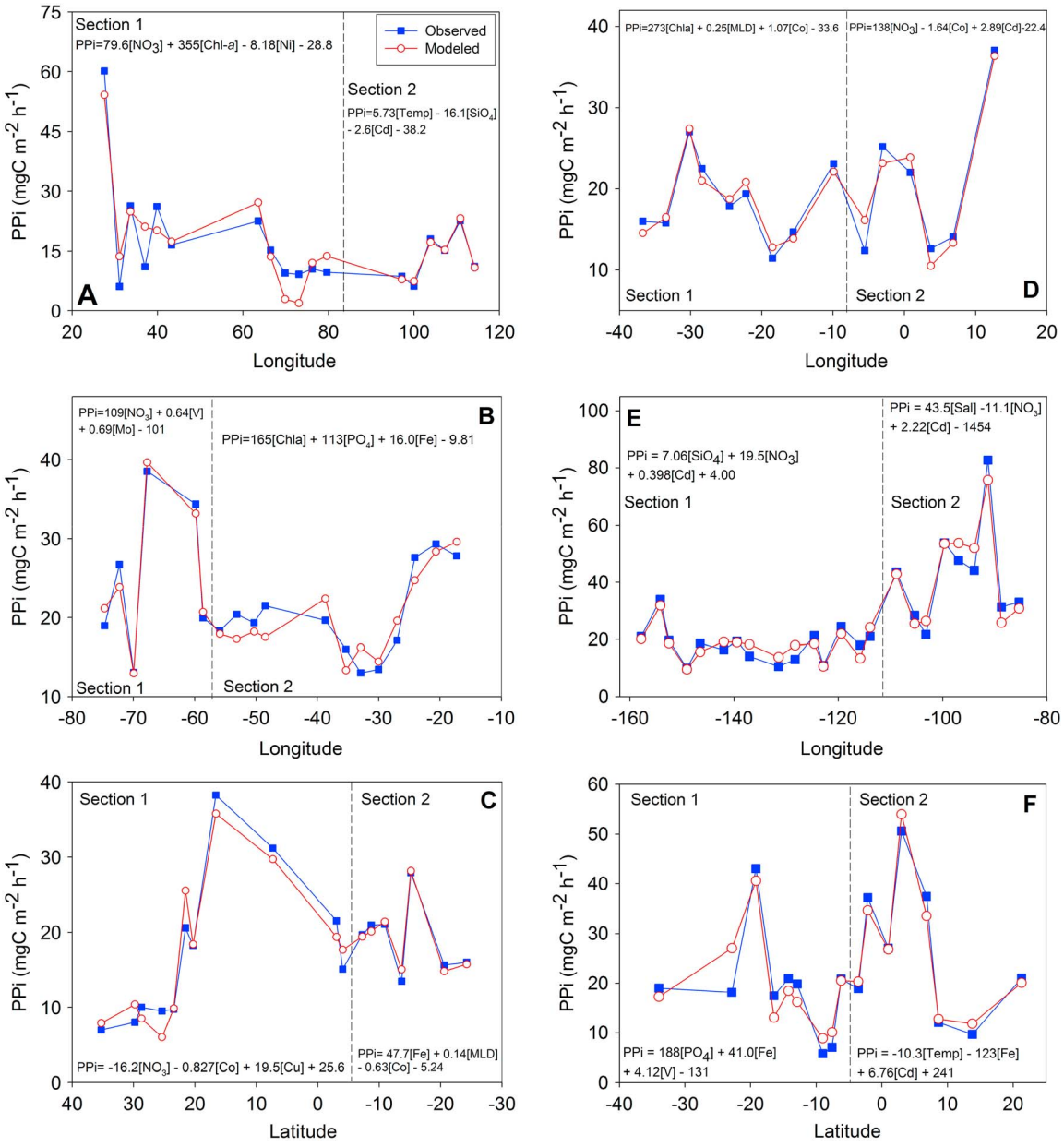

Figure 10. Observed versus modeled primary productivity (PPi) for the transect from (a) South Africa to Australia, (b) Colombia to Spain, (c) Spain to Brazil, (d) Brazil to South Africa, (e) Hawaii to Panama, and (f) New Zealand to Hawaii. The graphed model for each transect is that with the highest R^2, lowest p value, and lowest predictive error (Table 1). Formulas are given for each regression. Vertical dashed line separates different sections (see sections in Figure 1). Sections were determined on the basis of distinct hydrographic and biological regimes and tested by *k*-means cluster analysis.

Although the variables statistically determining primary productivity during the MCE were different for the different regions sampled, NO_3 comes out as an important parameter describing primary productivity in most ocean basins (Table 2), which is consistent with the low dissolved inorganic N:P ratios (Table S4) and the established notion that most of the global ocean is nitrogen limited [*Ryther and Dunstan*, 1971; *Falkowski*, 1997; *Moore et al.*, 2013]. The exception to this trend was observed in the transect from New Zealand to Hawaii, the only transect in which NO_3 is not required as an independent variable in the best fit model for primary productivity. This result is consistent with the fact that this transect crossed a zone of increased NO_3 concentrations—the Pacific Equatorial Divergence province [*Longhurst*, 1998]—and with recent work showing that primary productivity in this area of the Pacific Ocean has increased in recent decades due to a shift in phytoplankton community structure from mostly eukaryotes to mostly nitrogen-fixing

prokaryotes [*Karl et al*., 2001; *Sherwood et al*., 2014]. For the same transect, Table 2 shows that PO_4 and Fe are elements influencing primary productivity in this area of the ocean. This result is consistent with studies showing that both Fe [e.g., *Rueter et al*., 1992; *Falkowski*, 1997; *Wu et al*., 2000] and phosphorus [*Sañudo-Wilhelmy et al*., 2001] availability are primary factors limiting nitrogen fixation in the oceans, so the presence of these metal micronutrients in the best fit model agrees well with those studies.

Our model results also show that the lesser studied trace metal V is included as an important variable in some of the primary productivity models. Although the biological role for this element is not well characterized, high concentrations of V in field-collected Trichodesmium colonies have been observed [*Tovar-Sanchez and Sañudo-Wilhelmy*, 2011; *Nuester et al*., 2012], suggesting that V is enriched for N_2-fixing organisms. Furthermore, employing linear regression modeling of the North East Atlantic spring bloom, *Klein et al*. [2013] suggested that V might be linked to the removal of reactive oxygen species via V-haloperoxidases and/or passive uptake as an analog of PO_4^{3-} during P-limited conditions. It has also been shown that V enhances chlorophyll *a* biosynthesis by stimulating the synthesis of the porphyrin precursor 6-aminolevulinic acid (ALA), where V catalyzes the nonenzymatic transamination of 4.5-dioxovaleric acid to ALA [*Meisch and Bielig*, 1975, 1980]. In addition, *Meisch and Bielig* [1975] showed that V has the ability to overcome Fe deficiency in chlorophyll synthesis in some algal cells. The results of the multivariable linear regression modeling presented here are consistent with these previous studies, as the two transects that have V in the best fit model (Table 2) also include Fe and PO_4, nutrients that have the potential to limit nitrogen fixation in the ocean [*Rueter et al*., 1992; *Falkowski*, 1997; *Wu et al*., 2000; *Sañudo-Wilhelmy et al*., 2001]. Additionally, the inclusion of Fe in these models also supports the findings of *Meisch and Bielig* [1975] that the effect of V in the biosynthesis of chlorophyll *a* significantly increases in Fe-limited environments. This result is of particular interest, as the relationship between Fe, V, and the production of chlorophyll *a* in the open ocean is not well understood, meriting particular further attention.

The presence of SiO_4 in two of the best fit regression models (South Africa to Australia, and Hawaii to Panama) (Table 2 and Figures 10a and 10e) suggests that SiO_4 is a nutrient that may be controlling oceanic primary productivity in these areas of the ocean, where diatoms carry out the majority of the new production [*Dugdale and Wilkerson*, 1998], thus rendering SiO_4 a potential limiting nutrient. In fact, the North Tropical Pacific has been classified as a low-silicate, high-nutrient, low-chlorophyll *a* region because SiO_4 concentrations are not sufficiently high to support new production [*Dugdale and Wilkerson*, 1998]. Furthermore, the presence of Cd in all the best fit models that have SiO_4 as a variable (Table 2) agrees with culture and field measurements suggesting that Cd becomes biologically important for marine diatoms under conditions of low zinc [*Price and Morel*, 1990; *Lee and Morel*, 1995; *Lane and Morel*, 2000a, 2000b]. Although Zn levels were not determined for the MCE samples, it has been demonstrated that low zinc conditions are typical of open ocean environments [*Bruland*, 1989].

In general, the best fit models for all transects include metals other than Fe that may be important bioactive elements that can potentially limit or colimit oceanic primary productivity. For example, it has been reported that low Co concentrations in some regions of the world oceans limit the production of vitamin B_{12} by heterotrophic and phototrophic bacteria, especially in the North Atlantic Ocean [*Panzeca et al*., 2008]. The presence of Co in the best fit model for the northern section of the transect from Spain to Brazil (Table 1 and Figure 10c) agrees well with this previous study. Table 2 also shows that the metal micronutrients Ni and Mo were identified as elements influencing primary productivity in some of the sampled regions. It is well known that Mo plays an important role in the nitrogen cycle as a metal cofactor in nitrogenase [*Kisker et al*., 1997], and at least nine Ni-containing enzymes have been reported [*Mulrooney and Hausinger*, 2003]. However, gaps remain in our understanding of the biological role of these metals in the marine environment. Our linear regression modeling results could be used, with due caution in terms of functional inferences, as a tool in the design of future studies exploring unknown and potentially important roles for lesser studied trace metals.

4. Conclusions

The results reported here include dissolved Co, Fe Cd, Cu, Ni, V, and Mo distributions in surface waters of the global ocean, providing new data from unexplored regions of the ocean as well as for some understudied metals. By comparing our new data to previously published data sets on the distribution of trace metals in surface waters of the Atlantic Ocean (specifically the Spain to Brazil transect), we have explored changes in

the distribution of trace metals that have occurred in the last 30 years; for most metals, little change is observed over this time period. Multivariable linear regression modeling was used as a tool to describe relationships between primary productivity and the biogeochemical parameters measured during the MCE. Although caution must be taken in inferring causation from correlation models such as those presented here, this study suggests that some trace metal nutrients may have important biogeochemical roles by constraining, often in concert with macronutrients, algal biomass, and primary productivity. The results presented here point to the need of future experiments to verify a direct causal relationship between some of the lesser studied trace elements (e.g., Ni, V, Mo, and Cd) and oceanic primary productivity.

Acknowledgments
This research was partially supported by U.S. National Science Foundation (OCE 1435666), the USC Graduate School Dissertation Completion Fellowship, the Spanish Ministry of Economy and Competitiveness through the Malaspina 2010 expedition project (Consolider-Ingenio 2010, CSD2008-00077) and the project CTM2014-59244-C3-3-R. We thank Nick J. Klein for his help with the initial statistical analyses, Bieito Fernandez for the mixed layer depth data, L. Pinho, E. Mesa, H. Marota, and A. Dorsett for help with metal sampling, E. Fraile and V. Benitez for CTD data, M. Galindo for help with nutrient analyses, the UTM for help with the maintenance of the sampling system, and the captain and crew of R/V *Hesperides* for help during the circumnavigation. Data used to produce the results of this paper are available in the supporting information (Table S2).

References

Ammerman, J. W., R. R. Hood, D. A. Case, and J. B. Cotner (2003), Phosphorus deficiency in the Atlantic: An emerging paradigm in oceanography, *Eos Trans. AGU*, *84*, 165–170, doi:10.1029/2003EO180001.

Annett, A. L., S. Lapi, T. J. Ruth, and M. T. Maldonado (2008), The effects of Cu and Fe availability on the growth and Cu: C ratios of marine diatoms, *Limnol. Oceanogr.*, *53*, 2451–2461.

Berger, C. J., S. M. Lippiatt, M. G. Lawrence, and K. W. Bruland (2008), Application of a chemical leach technique for estimating labile particulate aluminum, iron, and manganese in the Columbia River plume and coastal waters off Oregon and Washington, *J. Geophys. Res.*, 113, C00B01, doi:10.1029/2007JC004703.

Bergquist, B. A., and E. A. Boyle (2006), Dissolved iron in the tropical and subtropical Atlantic Ocean, *Global Biogeochem. Cycles*, *20*, GB1015, doi:10.1029/2005GB002505.

Bertrand, E. M., M. A. Saito, J. M. Rose, C. R. Riesselman, M. C. Lohan, A. E. Noble, P. A. Lee, and G. R. DiTullio (2007), Vitamin B_{12} and iron colimitation of phytoplankton growth in the Ross Sea, *Limnol. Oceanogr.*, *52*, 1079–1093.

Bigg, G. R. (2003), *The Oceans and Climate*, Cambridge Univ. Press, Cambridge.

Blain, S., S. Bonnet, and C. Guieu (2008), Dissolved iron distribution in the tropical and sub tropical South Eastern Pacific, *Biogeosciences*, *5*, 269–280.

Bowie, A. R., D. J. Whitworth, E. P. Achterberg, R. F. C. Mantoura, and P. J. Worsfold (2002), Biogeochemistry of Fe and other trace elements (Al, Co, Ni) in the upper Atlantic Ocean, *Deep Sea Res., Part I*, *49*, 605–636.

Boyle, E. A., F. R. Sclater, and J. M. Edmond (1977), The distribution of dissolved copper in the Pacific, *Earth Planet. Sci. Lett.*, *37*, 38–54.

Boyle, E. A., S. S. Huested, and S. P. Jones (1981), On the distribution of copper, nickel, and cadmium in the surface waters of the North Atlantic and North Pacific Ocean, *J. Geophys. Res.*, *86*, 8048–8066, doi:10.1029/JC086iC09p08048.

Boyle, E. A., B. A. Bergquist, R. A. Kayser, and N. Mahowald (2005), Iron, manganese, and lead at Hawaii Ocean Time-series station ALOHA: Temporal variability and an intermediate water hydrothermal plume, *Geochim. Cosmochim. Acta*, *69*, 933–952.

Bristow, C. S., K. A. Hudson-Edwards, and A. Chappell (2010), Fertilizing the Amazon and equatorial Atlantic with West African dust, *Geophys. Res. Lett.*, *37*, L14807, doi:10.1029/2010GL043486.

Bruland, K. W. (1980), Oceanographic distributions of cadmium, zinc, nickel, and copper in the North Pacific, *Earth Planet. Sci. Lett.*, *47*, 176–198.

Bruland, K. W. (1989), Complexation of zinc by natural organic ligands in the central North Pacific, *Limnol. Oceanogr.*, *34*, 269–285.

Bruland, K. W., K. H. Coale, and L. Mart (1985), Analysis of seawater for dissolved cadmium, copper and lead: An intercomparison of voltammetric and atomic absorption methods, *Mar. Chem.*, *17*, 285–300.

Bruland, K. W., K. J. Orians, and J. P. Cowen (1994), Reactive trace metals in the stratified central North Pacific, *Geochim. Cosmochim. Acta*, *58*, 3171–3182.

Bruland, K. W., E. L. Rue, G. J. Smith, and G. R. DiTullio (2005), Iron, macronutrients and diatom blooms in the Peru upwelling regime: Brown and blue waters of Peru, *Mar. Chem.*, *93*, 81–103.

Canty, A., and B. Ripley (2014), Boot: Bootstrap, R (S-Plus) Functions. R package version 1.2-43 Package 'boot'.

Coleman, J. E. (1992), Zinc proteins: Enzymes, storage proteins, transcription factors, and replication proteins, *Annu. Rev. Biochem.*, *61*, 897–946.

Collier, R. W. (1985), Molybdenum in the Northeast Pacific Ocean, *Limnol. Oceanogr.*, *30*, 1351–1354.

Crans, D. C., J. J. Smee, E. Gaidamauskas, and L. Yang (2004), The chemistry and biochemistry of vanadium and the biological activities exerted by vanadium compounds, *Chem. Rev.*, *104*, 849–902.

Da Silva, J. F., and R. J. P. Williams (1993), *The Biological Chemistry of the Elements: The Inorganic Chemistry of Life*, Clarendon Press, Oxford, U. K.

Donguy, J. R. (1994), Surface and subsurface salinity in the tropical Pacific Ocean relations with climate, *Prog. Oceanogr.*, *34*(1), 45–78.

Duce, R. A., and N. W. Tindale (1991), Atmospheric transport of iron and its deposition in the ocean, *Limnol. Oceanogr.*, *36*, 1715–1726.

Dugdale, R. C., and F. P. Wilkerson (1998), Silicate regulation of new production in the equatorial Pacific upwelling, *Nature*, *391*, 270–273.

Dupont, C. L., K. Barbeau, and B. Palenik (2008), Ni uptake and limitation in marine Synechococcus strains, *Appl. Environ. Microbiol.*, *74*, 23–31.

Dupont, V., Y. Auger, C. Jeandel, and M. Wartel (1991), Determination of vanadium in seawater by inductively coupled plasma atomic emission spectrometry using chelating resin column preconcentration, *Anal. Chem.*, *63*, 520–522.

Ermler, U., W. Grabarse, S. Shima, M. Goubeaud, and R. K. Thauer (1998), Active sites of transition-metal enzymes with a focus on nickel, *Curr. Opin. Struct. Biol.*, *8*, 749–758.

Falkowski, P. G. (1997), Evolution of the nitrogen cycle and its influence on the biological sequestration of CO_2 in the ocean, *Nature*, *387*, 272–275.

Falkowski, P. G., and M. J. Oliver (2007), Mix and match: How climate selects phytoplankton, *Nat. Rev. Microbiol.*, *5*, 813–819.

Farmer, C. T., C. A. Moore, R. G. Zika, and R. J. Sikorski (1993), Effects of low and high Orinoco River flow on the underwater light field of the Eastern Caribbean Basin, *J. Geophys. Res.*, *98*, 2279–2288, doi:10.1029/92JC02764.

Feng, M., L. J. Majewski, C. B. Fandry, and A. M. Waite (2007), Characteristics of two counter-rotating eddies in the Leeuwin Current system off the Western Australian coast, *Deep Sea Res., Part II*, *54*, 961–980.

Field, C. B., M. J. Behrenfeld, J. T. Randerson, and P. Falkowski (1998), Primary production of the biosphere: Integrating terrestrial and oceanic components, *Science*, *281*, 237–240.

Gordon, A. L., J. R. Lutjeharms, and M. L. Gründlingh (1987), Stratification and circulation at the Agulhas Retroflection, *Deep Sea Rese. Part A. Oceanogr. Res. Pap.*, *34*, 565–599.

Grasshoff, K., K. Kremling, and M. Ehrhardt (2009), *Methods of Seawater Analysis*, John Wiley, New York.

Griffin, D. A., J. L. Wilkin, C. F. Chubb, A. F. Pearce, and N. Caputi (2001), Ocean currents and the larval phase of Australian western rock lobster, Panulirus cygnus, *Mar. Freshwater Res.*, *52*, 1187–1199.

Jia, Y., P. H. R. Calil, E. P. Chassignet, E. J. Metzger, J. T. Potemra, K. J. Richards, and A. J. Wallcraft (2011), Generation of mesoscale eddies in the lee of the Hawaiian Islands, *J. Geophys. Res.*, *116*, C11009, doi:10.1029/2011JC007305.
Karl, D. M., R. R. Bidigare, and R. M. Letelier (2001), Long-term changes in plankton community structure and productivity in the North Pacific Subtropical Gyre: The domain shift hypothesis, *Deep Sea Res., Part II*, *48*, 1449–1470.
Kisker, C., H. Schindelin, and D. C. Rees (1997), Molybdenum-cofactor-containing enzymes: Structure and mechanism, *Annu. Rev. Biochem.*, *66*, 233–267.
Klein, N. J., A. J. Beck, D. A. Hutchins, and S. A. Sañudo-Wilhelmy (2013), Regression modeling of the North East Atlantic Spring Bloom suggests previously unrecognized biological roles for V and Mo, *Front. Microbiol.*, *4*, 45.
Kremling, K. (1985), The distribution of cadmium, copper, nickel, manganese, and aluminium in surface waters of the open Atlantic and European shelf area, *Deep Sea Res., Part A*, *32*, 531–555.
Lane, T. W., and F. M. Morel (2000a), Regulation of carbonic anhydrase expression by zinc, cobalt, and carbon dioxide in the marine diatom Thalassiosira weissflogii, *Plant Physiol.*, *123*, 345–352.
Lane, T. W., and F. M. Morel (2000b), A biological function for cadmium in marine diatoms, *Proc. Natl. Acad. Sci. U.S.A.*, *97*, 4627–4631.
Lee, J. G., and F. M. Morel (1995), Replacement of zinc by cadmium in marine phytoplankton, *Mar. Ecol. Prog. Ser.*, *127*, 305–309, doi:10.3354/meps127305.
Lindskog, S. (1997), Structure and mechanism of carbonic anhydrase, *Pharmacol. Ther.*, *74*, 1–20.
Longhurst, A. R. (1998), *Ecological Geography of the Sea*, Academic Press, San Diego, Calif.
Lumley, T. (2009), Leaps: Regression subset selection. R package version 2.9 R Project for Statistical Computing, Vienna, Austria. [Available at cran.r-project.org/doc/packages/leaps.pdf.]
Maenhaut, W., H. Raemdonck, A. Selen, R. Van Grieken, and J. W. Winchester (1983), Characterization of the atmospheric aerosol over the eastern equatorial Pacific, *J. Geophys. Res.*, *88*, 5353–5364, doi:10.1029/JC088iC09p05353.
Marañón, E., P. M. Holligan, M. Varela, B. Mouriño, and A. J. Bale (2000), Basin-scale variability of phytoplankton biomass, production and growth in the Atlantic Ocean, *Deep Sea Res., Part I*, *47*, 825–857.
McClymont, E. L., R. S. Ganeshram, L. E. Pichevin, H. M. Talbot, B. E. Dongen, R. C. Thunell, A. M. Haywood, J. S. Singarayer, and P. J. Valdes (2012), Sea-surface temperature records of Termination 1 in the Gulf of California: Challenges for seasonal and interannual analogues of tropical Pacific climate change, *Paleoceanography*, *27*, PA2202, doi:10.1029/2011PA002226.
Meisch, H. U., and H. J. Bielig (1975), Effect of vanadium on growth, chlorophyll formation and iron metabolism in unicellular green algae, *Arch. Microbiol.*, *105*, 77–82.
Meisch, H. U., and H. J. Bieling (1980), Chemistry and biochemistry of vanadium, *Basic Res. Cardiol.*, *75*, 413–417.
Moore, C. M., et al. (2009), Large-scale distribution of Atlantic nitrogen fixation controlled by iron availability, *Nat. Geosci.*, *2*, 867–871.
Moore, C. M., et al. (2013), Processes and patterns of oceanic nutrient limitation, *Nat. Geosci.*, *6*, 701–710.
Moore, T. S., R. J. Matear, J. Marra, and L. Clementson (2007), Phytoplankton variability off the Western Australian Coast: Mesoscale eddies and their role in cross-shelf exchange, *Deep Sea Res., Part II*, *54*, 943–960.
Morel, F. M., and N. M. Price (2003), The biogeochemical cycles of trace metals in the oceans, *Science*, *300*, 944–947.
Morel, F. M., A. J. Milligan, and M. A. Saito (2006), Marine Bioinorganic Chemistry: The Role of Trace Metals in the Oceanic Cycles of Major Nutrients, *Oceans Mar. Geochem.*, *6*, 113.
Moreno-Ostos, E. (2012), Libro blanco de métodos y técnicas de trabajo oceanográfico, in *Proceeding of Expedición de Circunnavegación MALASPINA 2010 (Cambio Global y Exploración de la Biodiversidad del Océano)*, CSIC, Madrid, Spain.
Mulrooney, S. B., and R. P. Hausinger (2003), Nickel uptake and utilization by microorganisms, *FEMS Microbiol. Rev.*, *27*, 239–261.
Nuester, J., S. Vogt, M. Newville, A. B. Kustka, and B. S. Twining (2012), The unique biogeochemical signature of the marine diazotroph trichodesmium, *Front. Microbiol.*, *3*, 150.
Nürnberg, H. W., L. Mart, H. Rützel, and L. Sipos (1983), Investigations on the distribution of heavy metals in the Atlantic and Pacific Oceans, *Chem. Geol.*, *40*, 97–116.
Panzeca, C., A. J. Beck, K. Leblanc, G. T. Taylor, D. A. Hutchins, and S. A. Sañudo-Wilhelmy (2008), Potential cobalt limitation of vitamin B_{12} synthesis in the North Atlantic Ocean, *Global Biogeochem. Cycles*, *22*, GB2029, doi:10.1029/2007GB003124.
Peers, G., and N. M. Price (2006), Copper-containing plastocyanin used for electron transport by an oceanic diatom, *Nature*, *441*, 341–344.
Peers, G., S. A. Quesnel, and N. M. Price (2005), Copper requirements for iron acquisition and growth of coastal and oceanic diatoms, *Limnol. Oceanogr.*, *50*, 1149–1158.
Peterson, C. L. (1960), The physical oceanography of the Gulf of Nicoya, Costa Rica, a tropical estuary, *Inter-Am. Trop. Tuna Comm. Bull.*, *4*, 137–216.
Peterson, R. G., and L. Stramma (1991), Upper-level circulation in the South Atlantic Ocean, *Prog. Oceanogr.*, *26*, 1–73.
Pohl, C., P. L. Croot, U. Hennings, T. Daberkow, G. Budéus, and M. R. Van Der Loeff (2011), Synoptic transects on the distribution of trace elements (Hg, Pb, Cd, Cu, Ni, Zn, Co, Mn, Fe, and Al) in surface waters of the Northern- and Southern East Atlantic, *J. Mar. Syst.*, *84*, 28–41.
Price, N. M., and F. M. Morel (1990), Cadmium and cobalt substitution for zinc in a marine diatom, *Nature*, *344*, 658–660.
R Core Team (2014), *R: A Language and Environment for Statistical Computing*, R Foundation for Statistical Computing, Vienna, Austria. [Available at http://www.R-project.org/.]
Rehder, D. (2000), Vanadium nitrogenase, *J. Inorg. Biochem.*, *80*, 133–136.
Ridley, D. A., C. L. Heald, and B. Ford (2012), North African dust export and deposition: A satellite and model perspective, *J. Geophys. Res.*, *117*, D02202, doi:10.1029/2011JD016794.
Rueter, J., D. A. Hutchins, R. W. Smith, and N. L. Unsworth (1992), Marine pelagic cyanobacteria: Trichodesmium and other diazotrophs, in *Iron nutrition of Trichodesmium*, pp. 289–306, Springer, Netherlands.
Ryther, J. H., and W. M. Dunstan (1971), Nitrogen, phosphorus, and eutrophication in the coastal marine environment, *Science*, *171*, 1008–1013.
Saito, M. A., and J. W. Moffett (2002), Temporal and spatial variability of cobalt in the Atlantic Ocean, *Geochim. Cosmochim. Acta*, *66*, 1943–1953.
Saito, M. A., E. M. Bertrand, S. Dutkiewicz, V. V. Bulygin, D. M. Moran, F. M. Monteiro, M. J. Follows, F. W. Valois, and J. B. Waterbury (2011), Iron conservation by reduction of metalloenzyme inventories in the marine diazotroph Crocosphaera watsonii, *Proc. Natl. Acad. Sci. U.S.A.*, *108*, 2184–2189.
Saito, M. A., M. R. McIlvin, D. M. Moran, T. J. Goepfert, G. R. DiTullio, A. F. Post, and C. H. Lamborg (2014), Multiple nutrient stresses at intersecting Pacific Ocean biomes detected by protein biomarkers, *Science*, *345*, 1173–1177.
Sankaranarayanan, R., A. C. Dock-Bregeon, B. Rees, M. Bovee, J. Caillet, P. Romby, C. S. Francklyn, and D. Moras (2000), Zinc ion mediated amino acid discrimination by threonyl-tRNA synthetase, *Nat. Struct. Mol. Biol.*, *7*, 461–465.

Sañudo-Wilhelmy, S. A., A. B. Kustka, C. J. Gobler, D. A. Hutchins, M. Yang, K. Lwiza, J. Burns, D. G. Capone, J. A. Raven, and E. J. Carpenter (2001), Phosphorus limitation of nitrogen fixation by Trichodesmium in the central Atlantic Ocean, *Nature*, *411*, 66–69.

SCOR Working Group (2007), GEOTRACES–An international study of the global marine biogeochemical cycles of trace elements and their isotopes, *Chem. Erde Geochem.*, *67*, 85–131.

Sherwood, O. A., T. P. Guilderson, F. C. Batista, J. T. Schiff, and M. D. McCarthy (2014), Increasing subtropical North Pacific Ocean nitrogen fixation since the Little Ice Age, *Nature*, *505*, 78–81.

Slemons, L. O., J. W. Murray, J. Resing, B. Paul, and P. Dutrieux (2010), Western Pacific coastal sources of iron, manganese, and aluminum to the Equatorial Undercurrent, *Global Biogeochem. Cycles*, *24*, GB3024, doi:10.1029/2009GB003693.

Sunda, W. G. (2012), Feedback interactions between trace metal nutrients and phytoplankton in the ocean, *Front. Microbiol.*, *3*, doi:10.3389/fmicb.2012.00204.

Syrett, P. J., and A. M. Peplinska (1988), The effect of nickel and nitrogen deprivation on the metabolism of urea by the diatom Phaeodactylum tricornutum, *British Phycol. J.*, *23*, 387–390.

Talley, L. D., G. L. Pickard, W. J. Emery, and J. H. Swift (2011), *Descriptive Physical Oceanography: An Introduction*, Academic Press, Boston, Mass.

Taylor, G. T., and C. W. Sullivan (2008), Vitamin B_{12} and cobalt cycling among diatoms and bacteria in Antarctic sea ice microbial communities, *Limnol. Oceanogr.*, *53*, 1862–1877.

Tovar-Sanchez, A., and S. A. Sañudo-Wilhelmy (2011), Influence of the Amazon River on dissolved and intra-cellular metal concentrations in Trichodesmium colonies along the western boundary of the sub-tropical North Atlantic Ocean, *Biogeosciences*, *8*, 217–225.

Tyrrell, T. (1999), The relative influences of nitrogen and phosphorus on oceanic primary production, *Nature*, *400*, 525–531.

Umatani, S., and T. Yamagata (1991), Response of the eastern tropical Pacific to meridional migration of the ITCZ: The generation of the Costa Rica Dome, *J. Phys. Oceanogr.*, *21*, 346–363.

Van Der Loeff, M. R., E. Helmers, and G. Kattner (1997), Continuous transects of cadmium, copper, and aluminum in surface waters of the Atlantic Ocean, 50°N to 50°S: Correspondence and contrast with nutrient-like behavior, *Geochim. Cosmochim. Acta*, *61*, 47–61.

Wikström, M. (2006), *Cytochrome Oxidase*, John Wiley, New York.

Wu, J., W. Sunda, E. A. Boyle, and D. M. Karl (2000), Phosphate depletion in the western North Atlantic Ocean, *Science*, *289*, 759–762.

Yentsch, C. S., and D. W. Menzel (1963), A method for the determination of phytoplankton chlorophyll and phaeophytin by fluorescence, *Deep Sea Res. Oceanogr. Abstr.*, *10*, 221–231.